Ablation Product Radiation from Cones

By William C. Davy, Roger A. Craig, Gary T. Chapman, and Dale L. Compton
Research Scientists, NASA Ames Research Center, Moffett Field, California

Introduction

In the study of radiation associated with hypersonic flight, it has been noted in several papers[1-5] that the ablation process is accompanied by an increase in radiation from the vehicle shock layer. This increase is attributed[1] to ablation products in the boundary layer which have diffused outward from the surface and attained a high enough temperature to emit optical radiation. A more complete understanding of the process of ablation product radiation is desirable and necessary because, as is indicated in reference 1, under certain conditions this radiation can be a substantial part of the heating of vehicles entering the atmosphere. In addition, since the ablation process is intimately coupled with the energy exchange mechanism in the boundary layer, an understanding of the ablation product radiation process may constitute a diagnostic tool for the study of atmospheric entry phenomena.

Recently, interest has been directed to conical shapes for atmospheric entry.[6] This interest arises from a need to reduce the over-all heating of a vehicle entering at hyperbolic speeds, at which the air radiation becomes excessive for a blunt vehicle. Since air radiation exhibits a strong temperature dependence, it is possible to reduce greatly the heating of the vehicle by air radiation and convection by using a conical shape. Moderately increased convective heating is accepted for greatly reduced air radiation; however, not considered thus far is the heating on a cone due to ablation product radiation, the presence of which may influence the minimization of total heating.

The purpose of the present paper is therefore to describe a method by which ablation product radiative characteristics deduced from tests of blunt models in free-flight ballistic ranges can be used to predict ablation product radiative heating on a cone. The predictions are arrived at through an analysis based upon an equation for the radiation per unit mass of ablated material. This equation assumes a simple dependence upon material and local values of temperature and density. The empirical constants in the equation are evaluated from computed boundary-layer properties on a blunt vehicle and from observations of ablation product radiation during ballistic tests of blunt models. The resulting information is applied to the analysis of the boundary-layer properties on an ablating cone to correlate and predict the ablation product radiation. The predictions are then compared with observations of ablation product radiation in ballistic-range tests of cones.

Symbols

C — boundary-layer edge velocity gradient, sec^{-1}

c_p — total specific heat

E — radiant output per unit mass, watts/gram

f — dimensionless stream function

g — ratio of local static enthalpy to the total enthalpy

H — total enthalpy

h — static enthalpy

h_{eff} — effective heat of ablation, joules/gram

J — local radiative power, watts/cm^3

K — radiation constant, watts $(\text{cm})^{3\zeta}(\text{gm})^{-(\zeta+1)}(^{\circ}\text{K})^{-\xi}$

K_c — convective heat-transfer constant, watts-cm$^{-3/2}$

k — total thermoconductivity

$\imath$ — $\rho\mu/\rho_w\mu_w$, where μ is the viscosity

$\dot{m}$ — mass injection rate per unit surface area, gm/cm^2-sec

$\dot{Q}_a$ — total radiating heating flux, watts

$\dot{q}$ — local heating rate, watts/cm^2

Re — Reynolds number based on boundary-layer edge condition and slant length

r — radius from line of symmetry to the location x on the surface, cm

Sc — Schmidt number

s — surface area, cm^2

T — temperature, $^{\circ}$K

u — velocity in x direction, km/sec

V — velocity, km/sec

V_d — diffusion coefficient

v — velocity in y direction, km/sec

W — mass fraction of ablation products in the boundary layer

x — distance along surface, measured from cone apex, cm

y — distance measured normal to surface, cm

z — transformed normal distance, $\rho_w\,dz = \rho\,dy$

γ — transformed length

ζ — exponential dependence of E on density

η — transformed distance normal to the wall

θ_c — half angle of cone

ξ	exponential dependence of E on temperature
ρ	density, gm/cm^3
σ	Prandtl number

Subscripts

b	base
e	edge of boundary layer
$\dot{m}=0$	condition of zero mass injection
w	wall

Analysis

The analysis by which the blunt-body ablation product radiation was correlated, and which is extended to cones in the present paper, is based on a consideration of the gross processes which occur in the laminar boundary layer. The initial assumption is made that the ablation products are gases, ejected from the surface, and are diffusing through the boundary layer. The radiant power output per unit mass of ablated material is assumed to have a power law dependence on temperature and density given by

$$E = K\rho^{\zeta}T^{\xi} \qquad (1)$$

where E is the power radiated per unit mass of ablated products (for units, see list of symbols), ρ and T are the total properties of the air-ablation product mixture, and the parameters K, ζ, and ξ are constants which depend only on ablation material. Note that any effects on ablation product radiation due to chemistry (species change, etc.) will appear especially in the magnitude of ζ. A ζ value of zero, for example, removes the density dependence from equation (1) and this infers that if there are chemical reactions present they either produce no change in ablation product radiation or are not density dependent.

A heating flux, $\dot{Q}_a$, is defined as the total radiant power due to ablation product radiation which is incident on the model surface. If the source is geometrically and optically a thin radiating boundary layer, then $\dot{Q}_a$ is obtained by integrating one-half the radiant power output from the boundary layer over the model surface; namely,

$$\dot{Q}_a = \frac{1}{2} \int_{surface} \int_0^{y_e} WE\rho \, dy \, ds \qquad (2)$$

where W is the mass fraction of the ablation products in the boundary-layer mixture, ρ is the total gas density (air and ablation products), both being functions of y, the distance normal to the ablating surface. Contributions to the integral are negligible beyond y_e, defined as the value of y where W is 0.5 percent of the wall value.

Blunt-Body Analysis

The application of equation (2) to the boundary layer of a blunt body and the use of test data

to evaluate the constants ζ, ξ, and K in equation (1) are described in detail in reference 1 and are briefly outlined below.

For blunt-body boundary layers, equation (2) may be integrated in closed form if several simplifying assumptions* are made. The most important of these are: (a) the velocity, temperature, and ablation product mass fraction are linear functions of the transformed normal distance from the wall, z, defined by

$$\rho \, dy = \rho_w \, dz \qquad (3)$$

(b) the variables all reach edge values at the same distance from the wall, and (c) the mass injection rate of ablation products is constant over the blunt face of the model. With these approximations and several other mathematical simplifications, equation (2) can be integrated in closed form to give

$$\dot{Q}_a = \frac{3sK\dot{m}\rho_e^{\zeta}T_e^{\xi+2}}{2C(\xi - \zeta + 1)(\xi - \zeta + 2)(T_e - T_w)^2} \qquad (4)$$

where s is the surface area of the model face, $\dot{m}$ is the mass injection rate, and C is the edge velocity gradient parallel to the surface. Measurements of $\dot{Q}_a$ obtained from observations of blunt models made of polycarbonate and polyethylene were correlated by use of equation (4) to obtain values of K and ζ. The approximate values so obtained are:

Polycarbonate: $K = 7 \times 10^{-8}$; $\zeta = 0$

Polyethylene: $K = 6 \times 10^{-7}$; $\zeta = 0.66$

Evaluation of ξ from the polycarbonate data gave 3.5 ±1, whereas insufficient variation of edge temperature for the polyethylene tests made meaningful determinations of ξ for polyethylene difficult. A value of 4.0 was used for convenience to correlate the data for both materials.

Figure 1 demonstrates how well the blunt-body data of reference 1 is correlated by equation (4) with the above values of the parameters. The factor T_e^{-4} appropriate for $\xi = 4$ and $T_w \ll T_e$ was used to reduce velocity dependence and allow a concise presentation over the velocity range of the data. The shaded regions in the figure represent equation (4) evaluated for a velocity range of 5 to 7 km/sec. The figure shows that the equations correlate the data to an accuracy of approximately ±50 percent. The fact that polyethylene ablation product radiation is more sensitive to changes in edge density is readily apparent, and this fact is reflected in the numerical magnitude of the density exponent. The reason the curves plotted in figure 1 do not exhibit slopes that compare with the value of ζ listed above (e.g., the curve for polycarbonate does not have zero slope) is that terms in equation (4) other than ρ_e^{ζ} have implicit density dependencies. The mass injection rate, $\dot{m}$, has a strong density dependence. For the

---

*The assumptions are based upon reasonable approximations of the boundary-layer processes on an ablating blunt body and are discussed in reference 1.

test conditions, for example, convective heating was the primary energy source causing ablation; thus the mass injection rate varies approximately as the square root of the boundary-layer-edge density.

Cone Analysis

To predict the ablation product radiation from boundary layers on cone-shaped bodies, equation (2) must be integrated with the appropriate boundary layer, temperature, density, and ablation product distributions, which are different from those on a blunt body. As will be shown, the distribution of temperature within the boundary layer on a conical body is so nonlinear that the simplifying linear approximations used in the blunt-body analysis can no longer be applied. To obtain the distributions of local values of temperature, concentration of ablation products, and density, it was necessary to obtain machine solutions of the differential equations for momentum, energy, and mass conservation in the boundary layer, with appropriate boundary values specified at the wall and at the boundary-layer edge. The major assumptions which were used to obtain these solutions are:

1. The boundary layer is thin (usual boundary-layer assumption[7]).

2. The injected material (ablation products) has the same state and transport properties as does equilibrium air with, of course, the exception that its radiative property is given by equation (1).

3. The state and transport properties of the gas are given by the calculations of Hansen.[8] (Note: The total thermal conductivity of Hansen is used as opposed to the partial conductivity.)

4. The radiative energy loss from the boundary layer is neglected (i.e., no radiative-convective coupling).

A complete description of the solutions of the boundary-layer equations for a cone is to be found in the appendix. A typical set of boundary-layer profiles resulting from these solutions is shown in figure 2. The figure shows the variation of the boundary-layer temperature and ablation product mass fraction with distance from the wall. Shown also are the same distributions for the blunt body, as calculated from the earlier blunt-body analysis.* The calculations are based on the model configurations, 30° half-angle for the cone, and nose radius-to-diameter ratio of 0.71 for the blunt body. The free-stream density and velocity are equal for both geometries. Note that the mass fraction distribution for both cases is nearly a linear function of distance from the wall. However, the temperature distributions are markedly different; the boundary layer of a cone is bounded by a much lower edge temperature and shows a small overshoot of this temperature within the layer.

The local value of the radiation in power per unit volume is given by the expression

---

*In converting the linear profiles of reference 1 to the form of figures 2 and 3, it was assumed that the state properties of the mixture boundary layer are those of equilibrium air.

$$J = WE\rho \propto W\rho^{\zeta+1}T^{\xi} \qquad (5)$$

The distribution of J, normalized by its maximum value, is shown in figure 3 for both configurations. The effect of the difference in the temperature distributions is clearly evident; the maximum radiation occurs at smaller values of y/y_e for a boundary layer on a cone as contrasted to that on a blunt body. Further, because of the positive value of the density exponent ζ, the maximum of the polyethylene radiation is shifted toward the wall for both geometries. The maximum level of J is indicated for each case. Since the areas under each curve are approximately equal, the heating flux per unit area for equal thickness boundary layers is approximately proportional to J_{max}. Thus it can be seen that the local ablation product radiation to the surface will be a factor of 5 to 10 higher (for polycarbonate and polyethylene, respectively) for the blunt body at equal flight conditions and at equal y_e. However, y_e increases from zero as $x^{1/2}$ for the cone and is essentially constant for the blunt body. For the case above, with the additional condition of base diameters of 1 centimeter for both geometries, the total ablation product radiation flux, $\dot{Q}_a$, is calculated as approximately a factor of 10 to 20 higher (polycarbonate and polyethylene, respectively) for the blunt body than for the cone.

The final form of equation (2) for a boundary layer on a conical body, as developed in the appendix, is

$$\dot{Q}_a = \left(\frac{4\pi}{5\sqrt{6}}\right)\frac{K\rho_e^{\zeta+1}\, T_e^{\xi} W_w \sin\theta_c x_b^3}{Re^{1/2} l_e^{1/2}}$$

$$\int_0^{\eta_e}\left(\frac{1-g}{1-g_w}\right)\left(\frac{T}{T_e}\right)^{\xi}\left(\frac{\rho}{\rho_e}\right)^{\zeta}d\eta \qquad (6)$$

where g is the ratio of local static enthalpy to the total enthalpy, Re is the Reynolds number based on slant length, $l = \rho\mu/\rho_w\mu_w$, μ is the viscosity, x_b is the slant length of the cone, and η is a transformed normal distance given by

$$\eta = \frac{u_e r}{\sqrt{2\gamma}}\int_0^y \rho\, dy$$

where

$$\gamma = \int_0^x \rho_w\mu_w u_e r^2\, dx$$

Experimental Apparatus

A small amount of data on ablation product radiation from cones was collected for comparison with the results of the analysis. The facility used was the Prototype Free-Flight Facility of the Ames Research Center. This facility is described in detail in reference 9. Models were launched by a light-gas gun into a test chamber containing air at various pressures. Radiometers and conventional ballistic-range shadowgraphs spaced along the test chamber provided data on radiant intensity, model velocity, and attitude. The tests covered a free-stream density range of 0.007 to 0.13 amagats, and were made at velocities of approximately 7 km/sec.

3

The models were 30° half-angle cones with a base diameter of 10 mm. The ablating models were made of polyethylene and polycarbonate (trade name, Lexan). Nonablating models made from aluminum were also tested. Tests of blunt-nose models were of a similar nature and are reported in reference 1. These tests cover a velocity range of 4.5 to 7.5 km/sec.

Eleven narrow-pass (typically 0.04 micron) radiometers were used to determine the spectral intensity of radiation from 0.2 to 1.1 microns. Each radiometer consisted basically of a multiplier phototube, a narrow-pass optical filter and two slits, as is shown schematically in figure 4. Slit width was chosen to allow observation of the radiation from the forebody shock layer without interference from wake radiation. Calibration of the radiometers and data-reduction procedure is described in detail in reference 1.

Data and Data Reduction

Figure 5 shows the general features of radiation about cones. The figure is a photograph of an ablating cone taken with an image-converter camera. The light source was the radiation in the vicinity of the model. The effect of the S-11 spectral response of the image converter and the transmission of the lens and test section window limits the responsive wavelength region to 0.39 to 0.65 micron and, as will be shown later, the major fraction of the radiation that falls into this spectral region is from ablation products. The figure is thus primarily a photograph of the radiating ablation products. The pattern of radiation is not symmetric because of slight angle of attack.

Figure 6 presents typical spectra of the observed radiation in watts per micron into 4π steradians, obtained from ablating and nonablating cones. The ablation material is polyethylene (the same general features are observed in spectra from ablating polycarbonate) and the nonablating model is a copper-tipped aluminum cone. These spectra are constructed by fairing curves through the data which are represented by the horizontal lines whose lengths indicate the 50-percent bandpass widths of the radiometers. The area under each line indicates total power viewed by each radiometer in its wavelength band. Included for reference is the spectrally responsive region of the image converter used to obtain the photograph presented previously in figure 5. For purposes of comparison, the maximum possible surface radiation contribution, multiplied by 100, is also presented in figure 6. The calculation of the surface contribution is based on an emissivity of one and a surface temperature of 1000° K.* It is apparent from the figure that the contribution of the surface radiation to the total radiation observed is insignificant. Further tests described in reference 1 show similar results for blunt bodies. Thus, the spectrum from the ablating model is considered to represent radiation from

*Approximately 1000° K is given for the surface temperature of ablating polyethylene in reference 10 and Messrs. T. Wentink, Jr., L. Isaacson, and G. Economou of AVCO Corp. have recently measured by photometric techniques the same temperature for ablating polycarbonate. The aluminum surface is limited to its melting temperature, 920° K. Hence, the estimate shown is roughly applicable to both types of models.

ablation products and from air in the shock layer, whereas the spectrum from the nonablating model represents radiation from the air in the shock layer alone. It can also be seen that the ablation product radiation is generally at wavelengths longer than 0.45 micron. It is apparent that the radiation contributed by the ablation products is comparable to that generated by air in the shock layer. A similar observation was made for blunt models in reference 1.

The observations of the radiation from the shock layer were converted to ablation product heating flux, $\dot{Q}_a$. To obtain the values of $\dot{Q}_a$ reported in this paper the spectra were integrated from 0.45 to 1.1 microns (the same spectral range used in ref. 1), multiplied by 2 because approximately one-half the radiation is blocked from view by the model and then divided by 2 because the surface intercepts approximately one-half the radiant energy. Ablation product radiation occurs beyond 1.1 microns;[2] hence, the data herein are considered to be lower limits.

A summary of data from similar blunt model tests is given in reference 1, whereas the following table gives a summary of data obtained from the cone model tests, together with other test parameters. Data were not included from cone tests where the angle of attack was greater than approximately 5°, since ablation product radiation was found to be sensitive to angle of attack.

Ablation material	V, km/sec	ρ_∞/ρ_o	$\dot{Q}_a$, watts	ρ_e/ρ_o	Re
Polyethylene	6.88	0.0066	0.2	0.062	0.05x10⁶
↓	7.16	.066	1.0	.60	.5x10⁶
	6.91	.13	1.6	1.2	1.0x10⁶
	6.61	.13	1.4	1.1	1.0x10⁶
Lexan	6.05	.12	30	1.0	0.8x10⁶

Comparison With Data From Cone Models

In this section the data taken during tests of ablating cones will be compared with predictions based upon the preceding analysis. To obtain the predictions, the temperature, density, and enthalpy distributions were calculated for several values of boundary-layer-edge density and free-stream velocity. Equation (6) was integrated and the radiation from both polycarbonate and polyethylene ablation products was calculated for the geometry of the conical test model. The results of the calculations are shown in figure 7 as the shaded regions. Here again $\dot{Q}_a$ has been divided by the fourth power of the boundary-layer-edge temperature, as indicated by equation (6) for $\xi = 4$. In computing the edge conditions for these predictions, it was assumed that the shock layer was in thermodynamic and chemical equilibrium. The figure shows that, within the framework of the assumptions of the analysis, ablation product radiation from the boundary layer on a conical model should have the same qualitative features as the radiation from the boundary layer on a blunt model; that is, the general level of the polycarbonate ablation product radiation is higher than that from polyethylene, while the density dependence of polyethylene radiation is larger than that of polycarbonate radiation.

Shown also in figure 7 are the ablation product radiative heating fluxes, $\dot{Q}_a$, measuring during

cone model tests. The Reynolds numbers of these tests were never greater than one million based on local flow properties and slant length, so that it is reasonable to expect laminar boundary layers. The data show agreement with the predicted values within a factor of 2. The one exception is a polyethylene data point obtained under low-density conditions such that the air behind the shock wave is noted to be substantially out of equilibrium from calculations made by Messrs. D. Eastman and C. Olson of Boeing Corp. The nonequilibrium condition leads to higher boundary-layer temperatures than were used in the predictions, which rely on an equilibrium air assumption; hence, a low predicted value is to be expected in this instance.

Concluding Remarks

It was shown by experiments performed as part of this study that one of the major components of radiation observed during flight of ablating cones at hypersonic speeds is due to ablation products present in the shock layer. The amount of ablation product radiation observed is a function of ablation material as well as flight parameters.

A method has been described for predicting the ablation product radiative heating from the boundary layer of a cone. The method relies on ablation properties deduced from study of a comparable blunt body. Predictions made by this method agree with measured values to within a factor of two for the two ablation materials investigated, polyethylene and polycarbonate. This agreement is significant because (1) the distributions of properties in the boundary layer of a cone are significantly different from those in the boundary layer on a blunt body, and (2) the average temperatures and densities in the cone boundary layer for the test conditions are lower by a factor of two than those for the blunt-body test conditions.

Because of the agreement between the cone tests and predictions, it appears that ablation product radiative heating fluxes on bodies of arbitrary shapes can be predicted if the appropriate boundary-layer quantities can be obtained.

Appendix

The radiative heating flux, $\dot{Q}_a$, from the ablation products in the boundary layer to the wall is given by equation (2) of the text as

$$\dot{Q}_a = \frac{1}{2} \int_{surface} \int_0^{y_e} WE\rho \, dy \, ds \qquad (A1)$$

where

$$E = K\rho^\zeta T^\xi \qquad (A2)$$

To integrate equation (A1) for the case of an ablating cone, W, ρ, and E must be specified in terms of the variable of integration. Thus the equations describing the appropriate boundary-layer flow must be formulated and solved.

The major assumptions used in defining the present model of the boundary layer with mass injection on a cone in equilibrium air are:

1. The usual thin boundary-layer assumptions[7]

2. The air state and transport properties are the total properties of the mixture[8] (i.e., they include the chemical reaction terms implicitly)

3. Radiative and convective energy coupling is neglected

4. The mass injected is gaseous and the state and transport properties are the same as equilibrium air, with the exception of the radiative property which is given by equation (A2).

Under these assumptions the boundary-layer equations are:

Conservation of mass:

$$\frac{\partial}{\partial y} (\rho u r) + \frac{\partial}{\partial x} (\rho v r) = 0 \qquad (A3)$$

Conservation of momentum:

$$\rho u \frac{\partial u}{\partial x} + \rho v \frac{\partial v}{\partial y} = \frac{\partial}{\partial y} \left(\mu \frac{\partial u}{\partial y} \right) \qquad (A4)$$

Conservation of energy:

$$\rho u \frac{\partial h}{\partial x} + \rho v \frac{\partial h}{\partial y} = \mu \left(\frac{\partial u}{\partial y} \right)^2 + \frac{\partial}{\partial y} \left(\frac{k}{c_p} \frac{\partial h}{\partial y} \right) \qquad (A5)$$

Diffusion equation:

$$\rho u \frac{\partial W}{\partial x} + \rho v \frac{\partial W}{\partial y} - \frac{\partial}{\partial y} \left(\rho V_d \frac{\partial W}{\partial y} \right) = 0 \qquad (A6)$$

Equation (A5) is more useful if combined with equation (A4) and rewritten in terms of the total enthalpy, H, as

$$\rho u \frac{\partial H}{\partial x} + \rho v \frac{\partial H}{\partial y} = \frac{\partial}{\partial y} \left(\frac{\mu}{\sigma} \frac{\partial H}{\partial y} \right) + \frac{\partial}{\partial y} \left[\frac{\mu}{2} \left(1 - \frac{1}{\sigma} \right) \left(\frac{\partial u}{\partial y} \right)^2 \right] \qquad (A7)$$

where σ is the Prandtl number. The boundary conditions for these equations are

$$\left. \begin{array}{l} \text{at } y = 0, \ u = 0, \ v = v_w, \ H = H_w, \text{ and } W = W_w \\ \text{as } y \to \infty, \ u \to u_e, \ H \to H_e, \text{ and } W \to 0 \end{array} \right\} \qquad (A8)$$

The boundary-layer model is now defined by equations (A3), (A4), (A6), and (A7) and boundary conditions, (A8).

The conservation equations are not coupled with the diffusion equation because of assumptions 2 and 4. Hence, equation (A6) may be solved subsequent to the following solution of the coupled equations (A4) and (A7).

The following transformations and variables are used:

Howarth transformation, $\quad \eta = \dfrac{u_e r}{\sqrt{2\gamma}} \displaystyle\int_0^y \rho \, dy$

$$(A9a)$$

Mangler transformation, $\gamma = \int_0^x \rho_w \mu_w u_e r^2 \, dx$ (A9b)

Dimensionless dependent variables,

$$f = \int f_\eta \, d\eta \,, \qquad f_\eta = \frac{u}{u_e} \,, \quad \text{and} \quad g = \frac{H}{H_e} \qquad (A10)$$

where variable subscripts indicate differentiation.

The differential equations transform to

$$(lf_{\eta\eta})_\eta + ff_{\eta\eta} = 2\gamma(f_\eta f_{\eta\gamma} - f_\gamma f_{\eta\eta}) \qquad (A11a)$$

$$\left(\frac{l}{\sigma} g_\eta\right)_\eta + fg_\eta + \frac{u_e^2}{H_e}\left[\left(1 - \frac{1}{\sigma}\right) lf_\eta f_{\eta\eta}\right]_\eta$$
$$= 2\gamma(f_\eta g_\gamma - f_\gamma g_\eta) \qquad (A11b)$$

$$\left(\frac{l}{Sc} W_\eta\right)_\eta + fW_\eta = 2\gamma(f_\eta W_\gamma - f_\gamma W_\eta) \qquad (A11c)$$

where $l = \rho\mu/\rho_w\mu_w$, $Sc = \mu/\rho V_d$, and the boundary conditions transform to

$$\left.\begin{aligned}&\text{at } \eta = 0, \; f_\eta = 0, \; f = f_w, \; g = g_w, \; \text{and } W = W_w\\&\text{and as } \eta \to \infty, \; f_\eta \to 1, \; g \to 1, \; \text{and } W \to 0\end{aligned}\right\} \quad (A12)$$

A stream function, ψ, defined to satisfy equation (A3) is given by

$$\frac{\partial\psi}{\partial y} = \rho ur \,, \qquad -\frac{\partial\psi}{\partial x} = \rho vr$$

and is used together with equation (A10) to obtain the value of f at the wall, the blowing parameter. The result is

$$f_w = -\frac{\int_0^x \dot{m}(x)r \, dx}{\sqrt{2\gamma}} \qquad (A13)$$

where $\dot{m}(x) = \rho_w v_w$ and is the rate of mass injection. For a simple ablation process the wall temperature is taken as constant and $\dot{m}$ is given by[11]

$$\dot{m}(x) = \frac{\dot{q}_c(x)}{h_{eff}} \qquad (A14)$$

where h_{eff} in the effective heat of ablation (assumed to be independent of heating rate) and $\dot{q}_c(x)$ is the cold wall convective heating with zero mass injection* and is given by, for the case of a cone (see eq. (A22)),

$$\dot{q}_c(x) = \frac{K_c(\rho_e,\theta_c,V,T_w)}{\sqrt{x}} \qquad (A15)$$

---

*The present analysis is based on convective heating. More generally, if other heating sources are to be considered, the equation for $\dot{m}(x)$ would be suitably modified.

It is easily shown that f_w is not a function of x. This result, together with the isothermal wall assumption and the equilibrium air assumptions, allow the right-hand sides of equations (A11) to be set to zero (i.e., similarity holds).

The relations resulting from setting equations (A11a) and (A11b) to zero were programmed and solved on a digital computer by a fourth-order Adams-Moulton procedure.[12] The equilibrium air properties, as correlated in reference 13, were used. Profiles of boundary-layer properties were generated and a typical temperature profile is shown in figure 2. This figure shows the characteristic overshoot of temperature in the boundary layer of a cone.

Before equation (A1) is integrated, the mass concentration must be specified. This can be obtained by integration of equation (A11c), the transformed diffusion equation. However, a simple approximation, consistent with the degree of approximations used in obtaining the empirical constants in equation (A2) is obtained when we use the Crocco result, namely, $Sc = 1$ and $\sigma = 1$. We can then write the ablation product mass fraction as

$$W = W_w\left(\frac{1 - g}{1 - g_w}\right) \qquad (A16)$$

which can be verified by substitution into equation (A11c) and comparison with equation (A11b). A similar approach could have been used to solve the transformed continuity equations, but the effect of setting the Prandtl number equal to unity would reduce or eliminate the overshoot in temperature. Since ablation product radiation is sensitive to the temperature (about T^4), this profile change could result in significant error in the evaluation of equation (A1). The ablation product mass fraction at the wall, required for analytical formulation of equation (A16), can be obtained if the net flow of air at the wall is zero. Analytically,

$$\rho_w V_d\left(\frac{\partial W}{\partial y}\right)_w + \rho_w v_w(1 - W_w) = 0 \qquad (A17)$$

which transforms to

$$W_{\eta_w} = Sc f_w(1 - W_w) \qquad (A18)$$

and can be solved by integration of equation (A11c) twice using equations (A11b) and (A17) with boundary conditions (A12). The result is

$$W_w = \left\{1 - \left[\frac{(f_{\eta\eta_w})^{Sc}}{Sc f_w \int_0^\infty \frac{(lf_{\eta\eta})^{Sc}}{l} \, d\eta}\right]\right\}^{-1} \qquad (A19)$$

Using the assumption $Sc = 1$ reduces (A19) to

$$W_w = \frac{1}{1 - (f_{\eta\eta_w}/f_w)} \qquad (A20)$$

We note that W_w is a function of the blowing parameter, f_w, and the shear stress parameter, f_{yy_w}. The shear stress parameter is obtained from solution of equations (A11a) and (A11b).

6

The total ablation product radiation heating flux may now be calculated from equation (A1), which is integrated once and transformed to yield

$$\dot{Q}_a = \left(\frac{4\pi}{5\sqrt{6}}\right)\frac{K\rho_e^{\zeta+1} T_e^{\xi} W_w \sin \theta_c x_b^3}{Re^{1/2} l_e^{1/2}}$$

$$\int_0^{\eta_e} \left(\frac{1 - g}{1 - g_w}\right)\left(\frac{\rho}{\rho_e}\right)^{\zeta}\left(\frac{T}{T_e}\right)^{\xi} d\eta \qquad (A21)$$

where

$$Re = \frac{\rho_e u_e x_b}{\mu_e}$$

The following is a description of the calculation procedures used to evaluate equation (A21). The steps were:

1. Machine solutions of equations (A11a) and (A11b) were obtained for a series of different blowing parameters, f_w, at specific flight conditions (i.e., free-stream velocity and density). The solutions provide profiles of g, the total enthalpy, ρ/ρ_0, the density ratio, T/T_e, the temperature ratio, and $f_{\eta\eta_w}$, the shear stress parameter.

2. The wall concentration of ablation products was calculated by means of equation (A20).

3. The radiative heating rate was calculated from equation (A21) and plotted as a function of the blowing parameter; a typical example is shown in figure 8.

4. The blowing parameter was calculated for specific materials at the same flight conditions as the preceding calculations.

To calculate the blowing parameter as a function of the flight variables, one must specify zero mass injection heating rates and effective heats of ablation as functions of these variables. The zero mass injection heating rates as calculated from solutions of (A11a) and (A11b) are given in reference 14. For a wall temperature of 1000° K, $(\dot{q}_c)_{\dot{m}=0}$ is given by

$$(\dot{q}_c)_{\dot{m}=0} = 0.704 \frac{k_w}{c_{p_w}} \sqrt{\frac{\rho_w u_e x}{\mu_w}} \frac{1}{x} (H_e - H_w)V^{-0.36} \qquad (A22)$$

where the units of the coefficient 0.704 are $(km/sec)^{0.36}$. The effective heats of ablation, as reported in reference 15, are:

Polyethylene: $\quad h_{eff} = 4660 j/gm + 0.5(H_e - H_w)$

$$(A23a)$$

Polycarbonate: $\quad h_{eff} = 2910 j/gm + 0.5(H_e - H_w)$

$$(A23b)$$

Substituting equations (A22) and (A23) in equation (A14) allows this expression to be used to integrate equation (A13) to obtain

$$f_w = -\frac{0.574(H_e - H_w)V^{-0.36}}{\sigma h_{eff}} \qquad (A24)$$

Typical examples of f_w for polycarbonate and polyethylene are shown in figure 9.

With the proper value of f_w for the flight condition and ablation material under consideration, the corresponding value of $\dot{Q}_a$ was obtained; thus the symbols in figure 8 represent the value of f_w for the indicated conditions and for an effective heat of ablation corresponding to polyethylene. This procedure was then repeated for a series of flight conditions to obtain a plot such as shown in figure 7.

References

1. Craig, Roger A., and Davy, William C.: Thermal Radiation From Ablation Products Injected Into a Hypersonic Shock Layer. NASA TN D-1978, 1963.

2. Sternberg, M., et al.: Preliminary Studies of the Effects of Ablation Contaminants of Radiation. General Motors Corp. TR62-209, 1962.

3. Canning, Thomas N., and Page, William A.: Measurements of Radiation from Flow Fields of Bodies Flying at Speeds Up to 13.4 Kilometers Per Second. Presented to the Fluid Mechanics Panel of AGARD, April 3-6, 1962.

4. Lemay, A.: Radiation Measurements From the Plasma Sheath Surrounding Hypersonic Projectiles. CARDE, TM 693/62, 1962.

5. Leverance, R. A.: A Comparison of the Visible Radiation From Projectile Materials at Velocities From 6000 to 8500 ft/sec. NOLTR 61-162, 1961.

6. Allen, H. J., Seiff, A., and Winovich, W.: Aerodynamic Heating of Conical Entry Vehicles at Speeds in Excess of Earth Parabolic Speed. NASA TR R-185, 1963.

7. Schlichting, Hermann: Boundary Layer Theory. McGraw-Hill Book Co., Inc., New York, 1955.

8. Hansen, C. Frederick: Approximations for the Thermodynamic and Transport Properties of High Temperature Air. NASA TR R-50, 1959.

9. Seiff, Alvin: A Progress Report on the Ames Hypervelocity Free-Flight Facilities and Some of the Current Research Problems Being Studied in Them. Presented at the AIAA National Summer Meeting, Los Angeles, Calif., June 17-20, 1963.

10. Vojvodich, N. S.: The Performance of Ablative Materials in a High-Energy, Partially Dissociated, Frozen Nitrogen Stream. NASA TN D-1205, 1962.

11. Georgiev, S., Hildalgo, H., and Adams, Mac C.: On Ablating Heat Shields for Satellite Recovery. Avco Everett Res. Lab. Rep. 65, 1959.

12. Hildebrand, F. B.: Introduction to Numerical Analysis. McGraw-Hill Book Co., Inc., N. Y., 1956.

13. Viegas, John R., and Howe, John T.: Thermo-
     dynamic and Transport Property Correlation
     Formulas for Equilibrium Air From 1000° K
     to 15,000° K. NASA TN D-1429, 1962.

14. Canning, Thomas N.: The Physics of Hyper-
     velocity Flight as it Affects the Design of
     Reentry Vehicles. Presented at the Ninth
     Anglo-American Conference, Montreal, Canada,
     Oct. 21-24, 1963.

15. Savin, Raymond C., Gloria, Hermilo R., and
     Dahms, Richard G.: The Determination of
     Ablative Properties of Materials in Free-
     Flight Ranges. NASA TN D-1330, 1962.
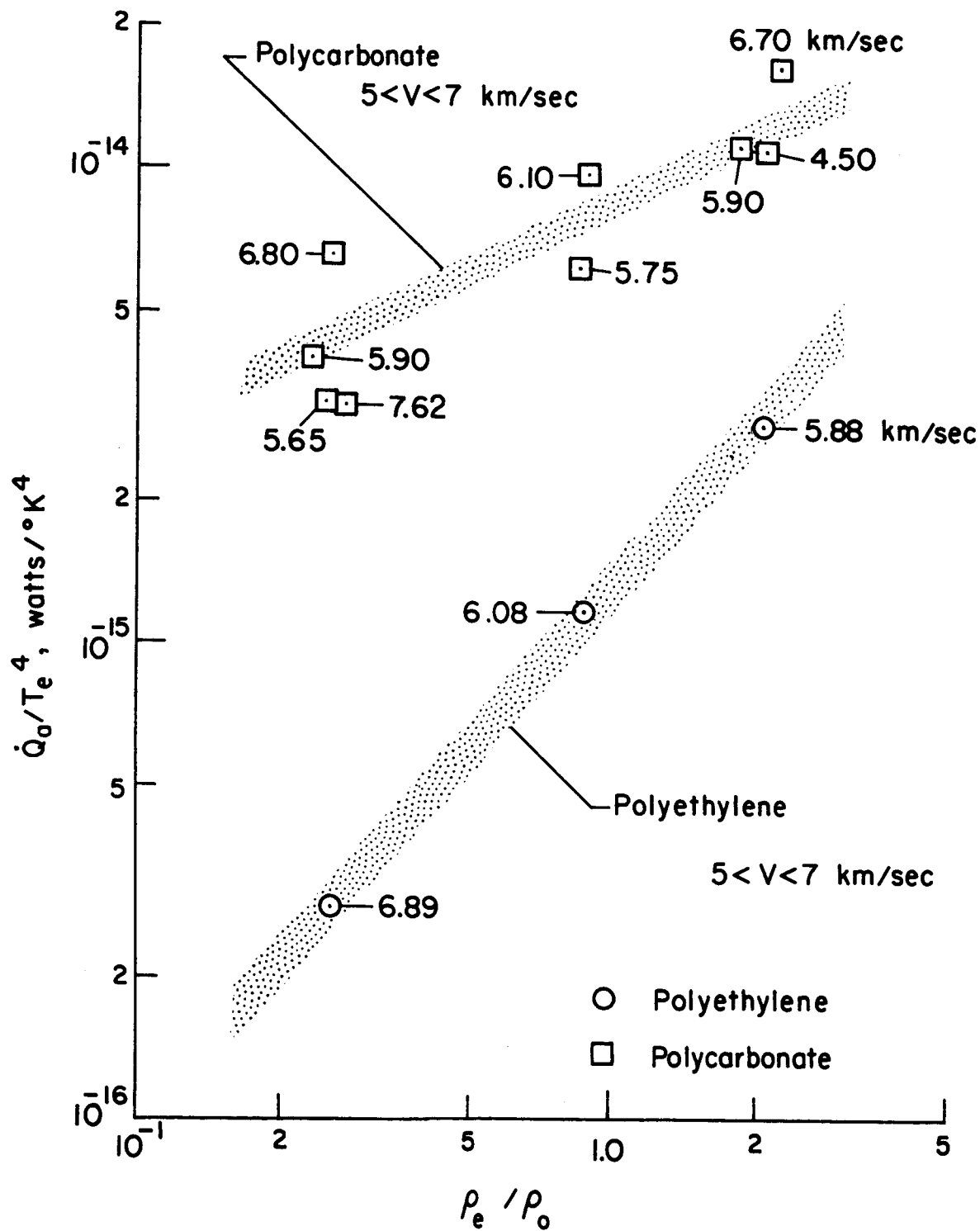
Figure 1.- Blunt-body data and correlating equation evaluated for
5 km/sec to 7 km/sec.
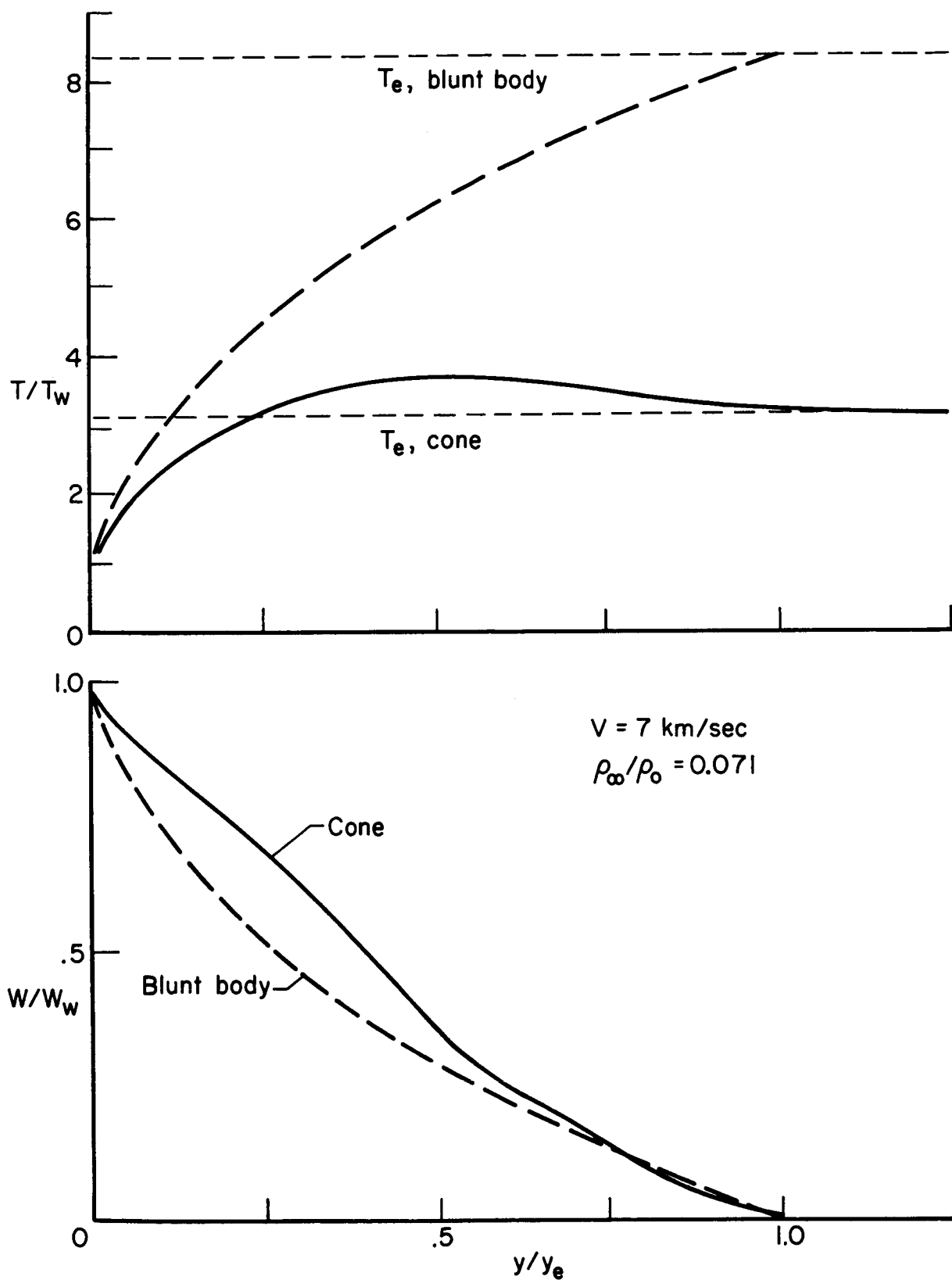
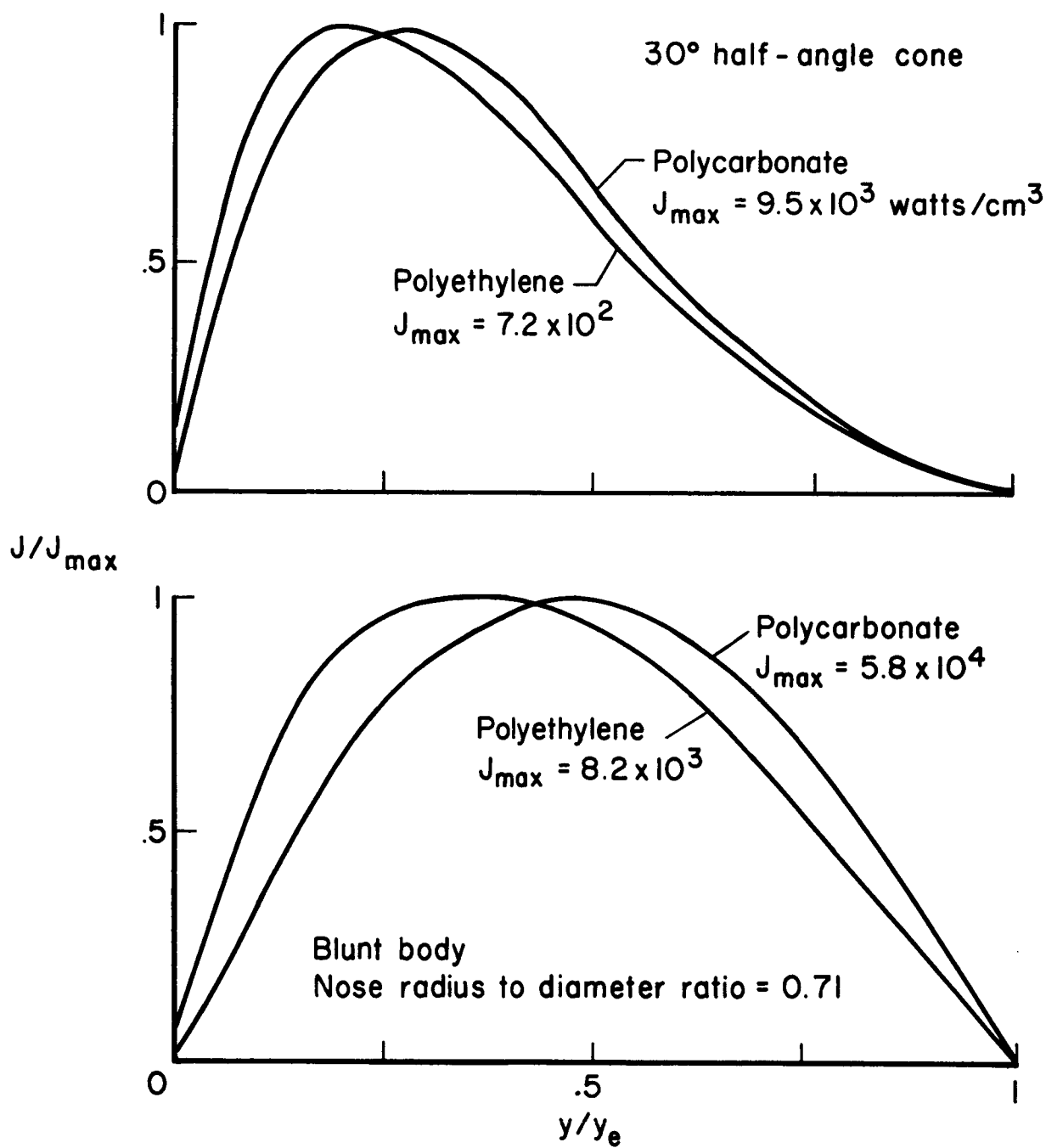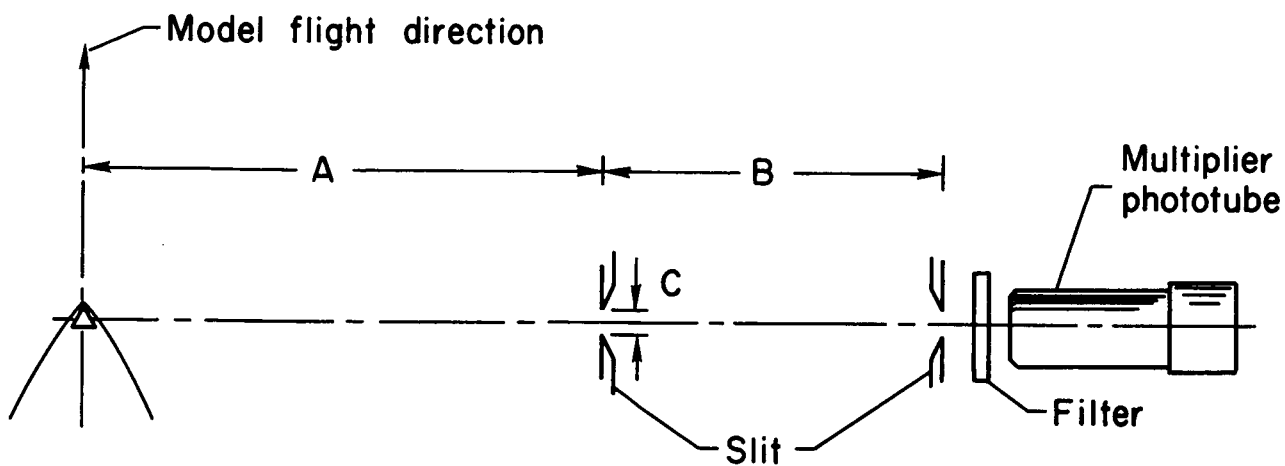Figure 2.- Boundary-layer profiles of temperature and ablation product concentration.

30° half-angle cone

Polycarbonate
$J_{max} = 9.5 \times 10^3$ watts/cm^3

Polyethylene
$J_{max} = 7.2 \times 10^2$

J/J_{max}

Polycarbonate
$J_{max} = 5.8 \times 10^4$

Polyethylene
$J_{max} = 8.2 \times 10^3$

Blunt body
Nose radius to diameter ratio = 0.71

y/y_e

Figure 3.- Profiles of local radiation in the boundary layer.

Figure 4.- Radiometer geometries.

The figure shows a radiometer geometry diagram with "Model flight direction" labeled at top, distances A, B, and C marked, a Slit, a Filter, and a Multiplier phototube.

	A	B	C
Blunt nose tests	9 cm	32 cm	10 mm
Cone tests	43 cm	38 cm	13 mm

$r_b = 0.51$ cm

1/2 angle = $30°$

Material:= polycarbonate

Exp. time = 0.5μ sec

V = 6.05 km/sec

$\rho_{\infty}/\rho_0 = 0.118$

$R_e = 0.8 \times 10^6$
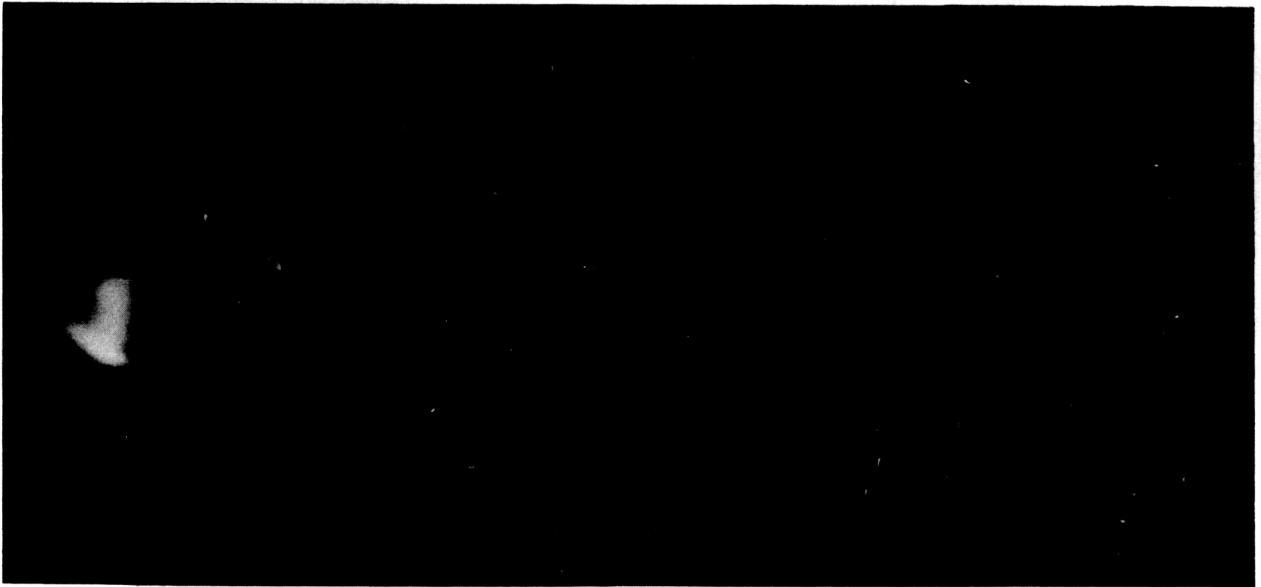
Figure 5.- Image-converter picture of an ablating cone.
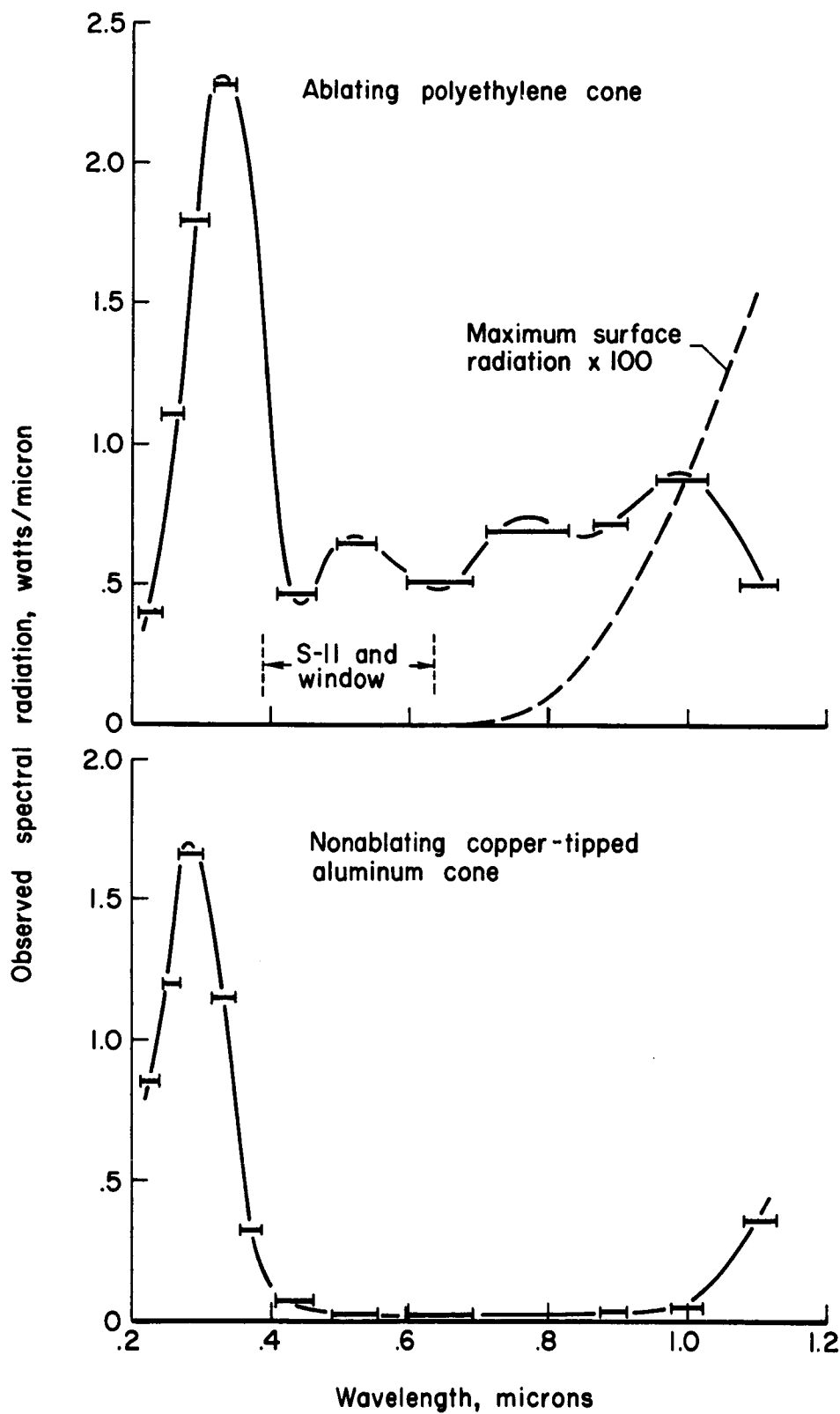
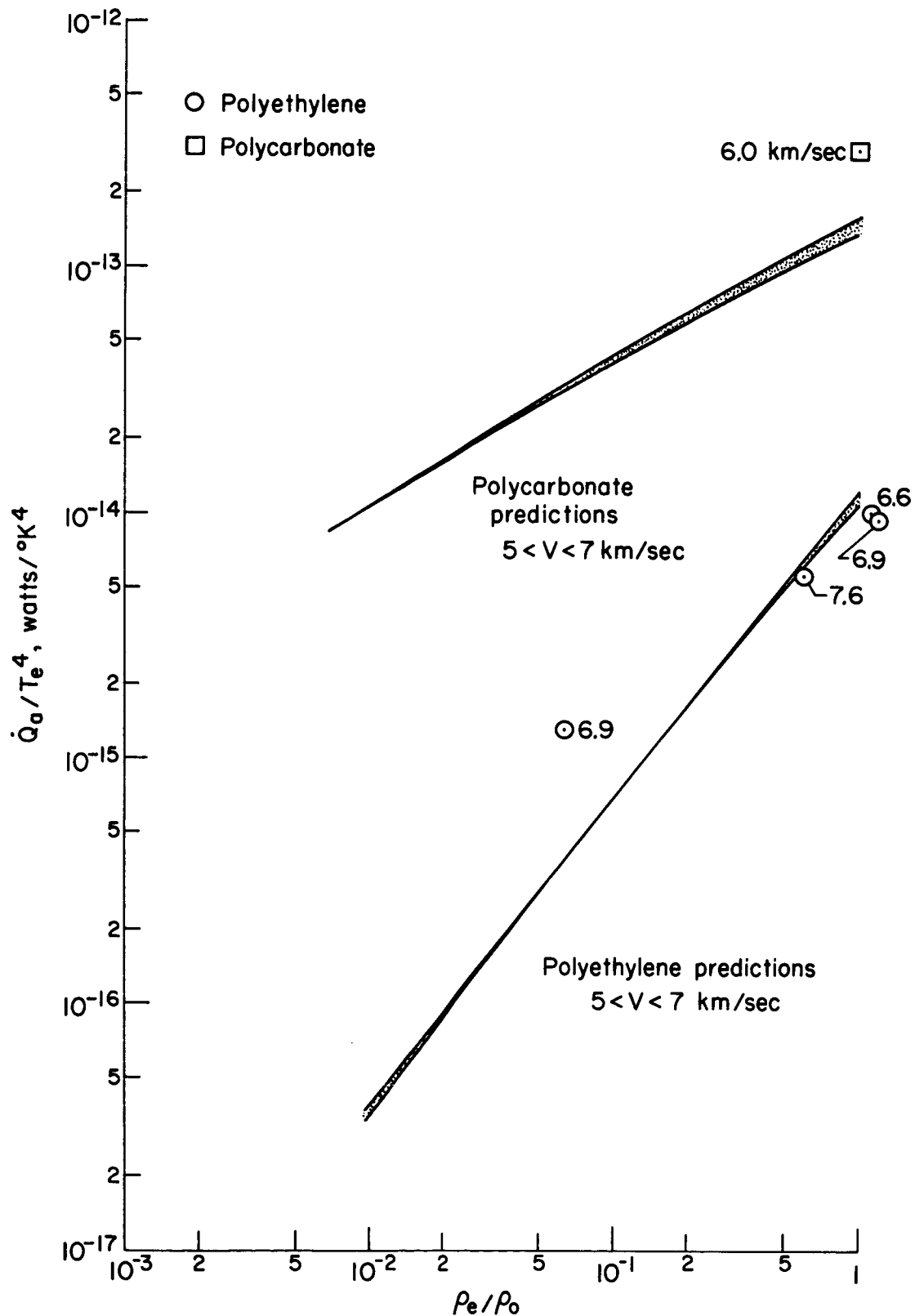Figure 6.- Examples of spectra; $V = 7.0$ km/sec, $\rho_\infty/\rho_0 = 0.013$.

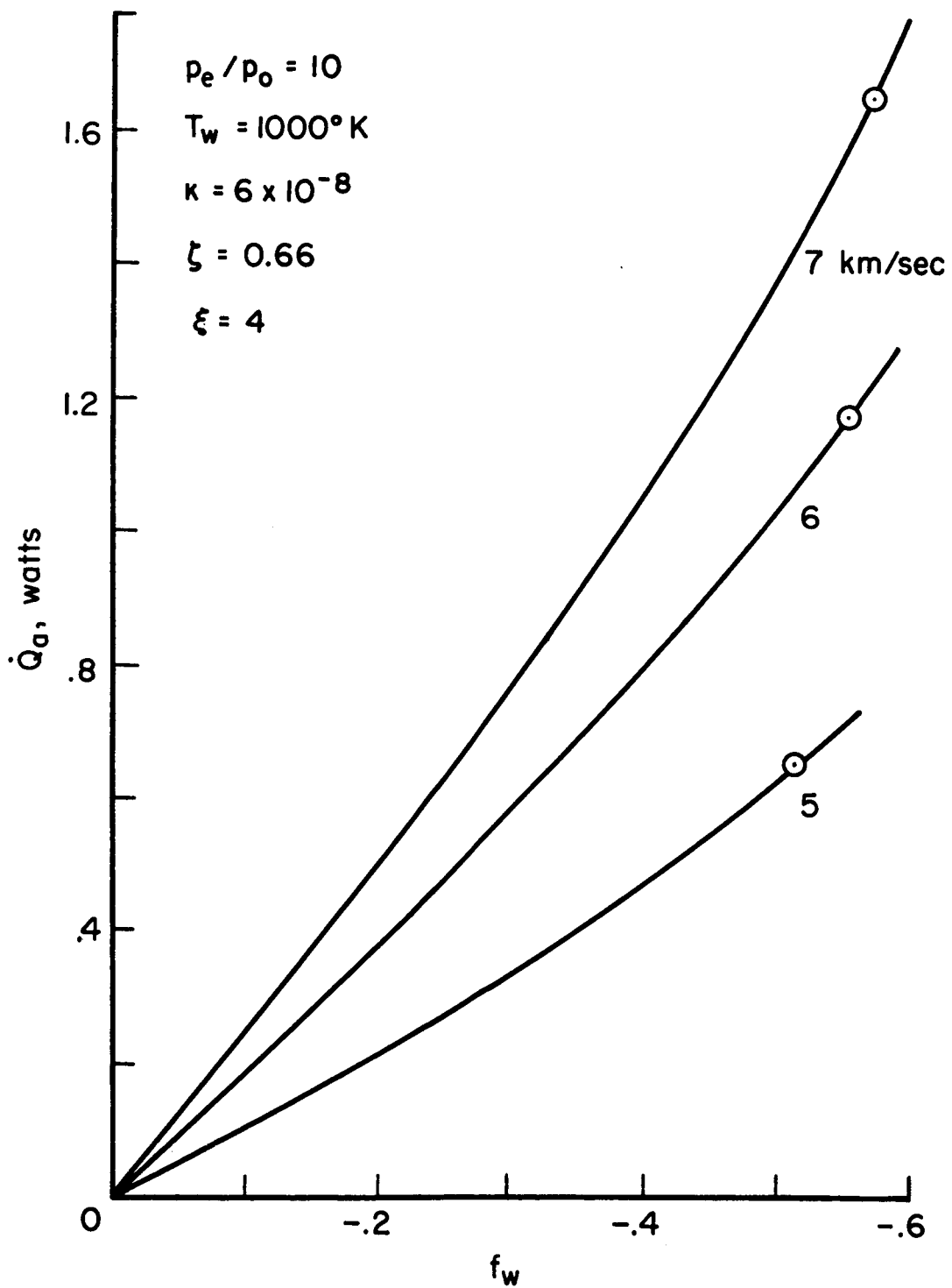Figure 7.- Comparison of cone data and predictions.

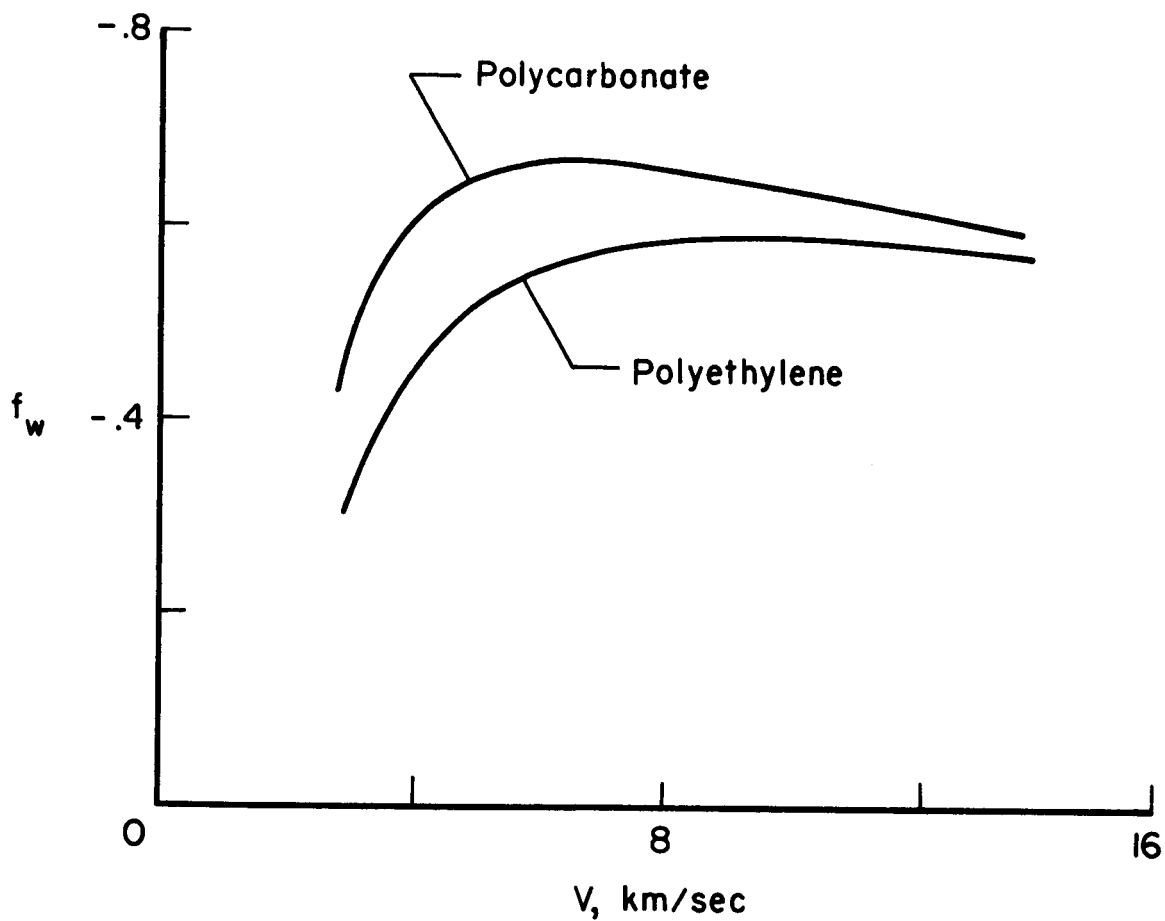Figure 8.- Ablation product radiative heating rates as a function of blowing parameter.

Figure 9.- Blowing parameter as a function of velocity.